Journal of Power Sources 196 (2011) 1333–1337

Contents lists available at ScienceDirect

Journal of Power Sources

journal homepage: www.elsevier.com/locate/jpowsour

Short communication

Simulation of coarsening in three-phase solid oxide fuel cell anodes

Hsun-Yi Chen [a], Hui-Chia Yu [a], J. Scott Cronin [b], James R. Wilson [b], Scott A. Barnett [b], Katsuyo Thornton [a,*]

[a] Department of Materials Science and Engineering, University of Michigan, 2300 Hayward St., Ann Arbor, MI 48109, USA
[b] Department of Materials Science and Engineering, Northwestern University, 2220 Campus Drive, Evanston, IL 60201, USA

ARTICLE INFO

Article history:
Received 13 July 2010
Received in revised form 9 August 2010
Accepted 10 August 2010
Available online 18 August 2010

Keywords:
Solid oxide fuel cell
Coarsening
Phase-field model
Three-phase boundary
Nickel
Yttria-stabilized zirconia

ABSTRACT

Coarsening of the nickel phase is known to occur in solid oxide fuel cell (SOFC) anodes consisting of Ni and yttria-stabilized zirconia (YSZ). However, the exact nature of the coarsening process is not known, nor how it affects three-phase boundaries (TPBs) and the resulting electrochemical performance. We apply a phase-field approach to simulate the microstructural evolution of Ni–YSZ anode functional layers. An experimentally obtained three-dimensional reconstruction of a functional layer from an anode-supported SOFC is used as the initial microstructure. The evolution of the microstructure is characterized quantitatively by examining the TPB density, interfacial area per unit volume, and tortuosity versus time. The assumed TPB contact angles are found to have a strong effect on the microstructural evolution; in particular, reducing the contact angle of nickel on YSZ yields less TPB reduction.

1. Introduction

Nickel particle agglomeration and coarsening have been considered major factors responsible for degradation in contemporary SOFCs with nickel–yttria-stabilized zirconia (Ni–YSZ) anodes [1]. Despite its importance, coarsening is difficult to investigate systematically because it proceeds slowly and must be examined over a long period of time. A few experiments of Ni coarsening can be found in the literature [2–4], but they do not examine the microstructures in three dimensions (3D), and thus it is difficult to characterize the evolution of tortuosities or connectivities of various phases [5]. There have been some modeling efforts as well, but these models are either statistical [6] or semi-empirical [3,7,8].

Ni coarsening in the SOFC anode is a capillarity-driven phenomenon. Regions with high curvatures have higher chemical potentials than those with lower curvatures in accordance with the Gibbs–Thomson effect, and thus the material will be transported from these regions to lower-curvature regions when mobility is sufficiently large for the time scale of interest. This leads to lower free energy of the system. The process can be formulated as a sharp-interface free-boundary problem, but it is difficult to numerically solve in 3D since explicit tracking of the interface is required. The phase-field model (PFM) handles the interface implicitly, where the interface information is embedded in field variables, often referred to as the order parameters (OPs). Immiscibility and interfacial energy are naturally incorporated in the PFM through the bulk free energy and the gradient energy penalty over the diffuse-interfacial region. The interfacial energy ratios among different interfaces can be specified in the PFM through proper parameterization of the free energy functional.

In this paper, we present two models to quantitatively simulate Ni coarsening. Our models are free from empirical fitting parameters when input kinetic and thermodynamic coefficients are known. Furthermore, to the best of our knowledge, this work is the first to perform coarsening simulations in 3D using an experimental microstructure of a Ni–YSZ anode.

2. Model formulation

To simplify our models, a few approximations have been made. First, the volume of each phase in the Ni–YSZ anode is assumed to be conserved (which is equivalent to mass conservation since the material is incompressible). (Note at ordinary operating temperatures of a SOFC (500–1000 °C), the evaporation of Ni is negligible [9].) Therefore, we apply the Cahn–Hilliard (conserved) equation as the governing equation. Second, the kinetic and thermodynamic properties are estimated at 1100 °C at which complementary experiments are conducted. In addition, Ni surface tension is assumed to be independent of crystal orientation, because its anisotropy is insignificant at this temperature [10]. For the surface diffusivity of Ni, we adopt the value measured from the mass transfer method, which can provide the mean value of multiple crystal facets and/or the value of certain facet of a single crystal [11].

* Corresponding author. Tel.: +1 734 615 1498; fax: +1 734 763 4788.
E-mail address: kthorn@umich.edu (K. Thornton).

0378-7753/$ – see front matter © 2010 Elsevier B.V. All rights reserved.
doi:10.1016/j.jpowsour.2010.08.010

We further simplify our models by identifying the dominant transport mechanism that dictates Ni coarsening in a Ni–YSZ anode. Three mechanisms play a role in the evolution of Ni microstructure: evaporation–condensation, bulk diffusion, and surface diffusion. The evaporation–condensation mechanism is negligible here due to the very low Ni vapor pressure [9]. Assuming atoms on the interface have similar values of chemical driving force for both surface and bulk diffusion (a quasi surface-volume equilibrium assumption), the ratio between surface diffusion and bulk diffusion contributing to the transport can be represented as $\sigma = D_s\delta_s/D_B w$, where D_s and D_B are surface and bulk diffusivities, respectively. Surface diffusion is considered to occur within the first several lattice layers on the surface within a thickness $\delta_s \sim 1$ nm. In the anode microstructural data we acquired, the characteristic length w of Ni particles falls between 0.1 and 1 μm. According to the literature, Ni surface diffusivity is on the order of 10^{-10} m^2 s^{-1} [10,11], while bulk diffusivity is of 10^{-16} m^2 s^{-1} at 1100 °C [12]. Therefore, the surface to bulk diffusion ratio is $\sigma \approx 10^3$ in this system, which suggests that surface diffusion dominates.

It is generally believed that the YSZ phase has very low mobility; that is, YSZ serves as the supporting structure in which Ni coarsens. Therefore, we may either allow YSZ to transport with its low mobility (Model A), or assume it to be immobile (Model B). The framework of these two PFMs will be discussed, and we will demonstrate that they lead to different coarsening kinetics.

2.1. Model A

In this model, we assume that the YSZ phase has a very small mobility, and consider the Ni–YSZ–pore anode as a system of three mobile phases. To model the phase evolution in a three-phase system with a PFM, three OPs, say ϕ_1, ϕ_2, and ϕ_3, may be required. However, by choosing the OPs to be the volume fraction of the corresponding phases, we eliminate one of the OPs through the constraint $\sum_{i=1}^{3}\phi_i = 1$. The governing equations then reduce to two coupled Cahn–Hilliard equations as

$$\frac{\partial\phi_i}{\partial t} = \nabla\cdot M(\phi_1,\phi_2,\phi_3)\nabla\frac{\delta\mathcal{F}}{\delta\phi_i}, \tag{1}$$

where $i = 1, 2$, $\mathcal{F}$ is the free energy functional, and M is a surface mobility function, described below. We utilize a Ginzburg–Landau-type free energy functional [13] of the form

$$\mathcal{F} = \int_V dV\left(\sum_{i=1}^{3}k_i\phi_i^2(1-\phi_i)^2 - \sum_{i,j=1,i>j}^{3}\alpha_{ij}^2\nabla\phi_i\nabla\phi_j\right). \tag{2}$$

This functional allows the control of interfacial energies and thicknesses of each type of interfaces through the selection of parameters k_i and α_{ij}. In addition, for unequal surface tensions, this functional leads to more computationally efficient evolution equations as compared to an alternative form of the free energy in Ref. [14]. The variational derivative of this functional can be calculated by the method of Lagrange Multipliers [14]. The interfacial energy $\gamma_{ij} = \alpha_{ij}\sqrt{(k_i+k_j)}/3$ and interfacial width $\delta_{ij} = \alpha_{ij}/\sqrt{(k_i+k_j)}$ for a planar interface between phases i and j can be found from the equilibrium solution. The model permits a small amount of the third phase to appear in a two-phase interface (as discussed in Ref. [14]), but it is limited to less than 3% in fraction.

The surface mobility function is taken to be

$$M(\phi_1,\phi_2,\phi_3) = \sum_{i,j=1,i>j}^{3}M_{ij}\prod_{C_l C_h}(\phi_i)\prod_{C_l C_h}(\phi_j)(\phi_i\phi_j(1-\phi_i)(1-\phi_j)), \tag{3}$$

where we introduced a boxcar function $\prod_{C_l C_h}(\phi_i)$, which takes a value of 1 when ϕ_i is between C_l and C_h and 0 otherwise, to avoid excess mobility resulting from the appearance of the foreign phase discussed above. Here, we set $C_l = 0.05$ as the lower cutoff OP value, and $C_h = 1 - C_l$ as the upper cutoff resulting from the complementary value of the lower cutoff.

To quantitatively link the simulation predictions to experiments, we performed an asymptotic analysis. Following Refs. [15,16], we obtain

$$\tau = K\frac{k_B T N_v L^4}{\delta_s\gamma_s D_s}, \tag{4}$$

where k_B and T are the Boltzmann constant and temperature. N_v, δ_s, γ_s, and D_s are the atomic number density, surface diffusion depth, surface energy, and surface diffusivity, respectively. L and τ are the characteristic length and characteristic time scale, respectively. K is approximately unity (equals 1.0147 for the simulations presented), determined by analytical integration, and it compensates for the aforementioned cutoff in the mobility function. The detailed derivation will be published in a forthcoming paper.

2.2. Model B

In this alternative model, we assume YSZ is stationary and therefore can be treated as the geometry within which Ni and pore phases evolve. We also assume that the Ni phase evolves via diffusion along Ni–pore interfaces, and the triple junction satisfies Young's equation for a contact angle with a locally flat surface. The dynamics of this system can thus be described by a single OP Cahn–Hilliard equation with two complementary boundary conditions (BCs): the contact-angle BC at triple junctions and no-flux BC at YSZ interfaces, where the OP distinguishes Ni and pore phases. We use the framework of the Smoothed Boundary Method (SBM) [19,20] and treat the contact-angle BC following Warren et al. [17,18].

For the standard Cahn–Hilliard dynamics, the evolution equation is

$$\frac{\partial\phi}{\partial t} = \nabla\cdot M\nabla\mu. \tag{5}$$

The chemical potential μ can be calculated as $\mu = \delta\mathcal{F}/\delta\phi = \partial f/\partial\phi - \varepsilon^2\nabla^2\phi$, where we use $\phi = 1$ as the Ni phase. The free energy functional in Model B has the standard form that consists of a double well potential and gradient energy penalty,

$$\mathcal{F} = \int_V dV\left[f(\phi) + \frac{\varepsilon^2\left|\nabla\phi\right|^2}{2}\right], \tag{6}$$

where $f(\phi) = W\phi^2(1-\phi)^2/4$. The SBM introduces a domain parameter ψ, which in this case distinguishes regions having YSZ ($\psi = 0$) and other phases ($\psi = 1$) as well as the YSZ interfaces ($0 < \psi < 1$). Like an ordinary OP in a phase-field approach, ψ varies continuously across the interface; thus, the unit interface normal $\vec{n}$ is given by $\vec{n} = \nabla\psi/\left|\nabla\psi\right|$. The contact angle θ at triple junctions dictated by Young's equation can be formulated as $\vec{n}\cdot\nabla\phi/\left|\nabla\phi\right| = -\cos\theta$.

The mechanical equilibrium at the triple junction corresponds to an extremum of the free energy, or $\delta\mathcal{F} = 0$. We can use the planar solution of the volume integration part of this extremum condition to find a useful equality, $\left|\nabla\phi\right| = \sqrt{2f}/\varepsilon$, which can be substituted into the aforementioned Young's condition to derive the SBM contact-angle BC as [17,21],

$$\nabla\psi\cdot\nabla\phi = -\left|\nabla\psi\right|\cos\theta\frac{\sqrt{2f}}{\varepsilon}. \tag{7}$$

This contact-angle BC only supplies energy on interfaces near triple junctions. The final evolution equation derived from SBM with no-

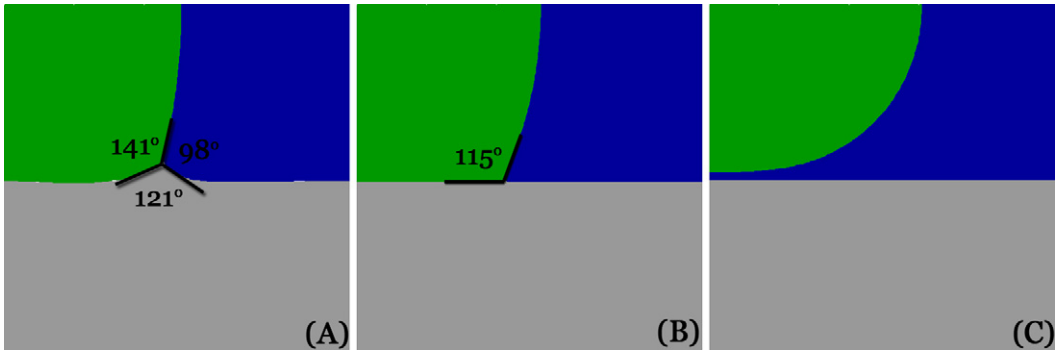

Fig. 1. A comparison of equilibrium contact angles at triple junctions with three different models; phases 1, 2, and 3 are represented in green, gray, and blue, respectively: (A) the result of Model A; (B) the result of Model B; (C) the result from evolving one order parameter in Model A. Note that the triple junction no longer exists at equilibrium in (C).

flux and contact-angle BCs is

$$\frac{\partial(\psi\phi)}{\partial t} = \nabla\cdot\left\{\psi M\nabla\left[f_\phi - \frac{\varepsilon^2}{\psi}\left(\nabla\cdot(\psi\nabla\phi) + \frac{|\nabla\psi|\sqrt{2f}}{\varepsilon}\cos\theta\right)\right]\right\}. \quad (8)$$

The mobility fuction in Model B is given by

$$M(\phi,\psi) = M_{\mathrm{Ni-pore}}\prod_{C_iC_h}(\phi)(\phi^2(1-\phi^2))g(\psi), \quad (9)$$

where $g(\psi) = \psi^6(10\psi^2 - 15\psi + 6)$ is introduced to control the mobility at and near triple junctions. The one-sided interpolation function $g(\psi)$ transits smoothly from 1 to the order of 0.01 as the domain parameter varies from 1 to 0.5. In this model, the mobility near a triple junction decreases by a factor of 10^{-6} as ψ varies from 1 to 0.1 along the Ni–pore interface.

3. Results and discussions

3.1. Contact angles at triple junctions

The mechanical equilibrium at a triple junction is examined in two dimensions with $\gamma_{13}:\gamma_{23}:\gamma_{12} = 1.9:1.4:2.2$ to validate our models. As shown in Fig. 1, the contact angles in both Model A and Model B are found to obey the Young's equation at equilibrium with different assumptions: in Model A, YSZ surface deforms near the TPB while in Model B, the YSZ is not allowed to deform.

A model one may consider is Model A (with two OPs) where one of the OPs is held constant after proper initialization. Such a model has been proposed and applied by others [8,13]. We find that this model would only work when the mobile phase completely wets the stationary phase as in Ref. [13], but not when three-phase boundaries are involved. In a PFM, the interfacial energy is controlled by the bulk and gradient energy coefficients, and an interface possesses the prescribed interfacial energy when the OP interfacial profile is in equilibrium (or near equilibrium when the interface is evolving). In Eq. (1), if one OP is held constant as proposed in [8], other OPs cannot develop their equilibrium profiles. This leads to contact angles at triple junctions that are inconsistent with the solutions of Young's equation. The full analysis of this problem is beyond the scope of this paper. Here, we simply demonstrate that the Young's condition is not met in Model A with one OP held constant, as shown in Fig. 1(C).

3.2. Effects of coarsening on microstructure and TPB density

Microstructures of SOFC anodes can be experimentally reconstructed [5]. We use an experimentally obtained Ni–YSZ anode microstructure of dimension 3.48 by 3.48 by 3.48 μm^3 (Fig. 2, left) as the initial condition for our coarsening simulations. For convenience, hereafter subscripts 1, 2, and 3 are used to represent the Ni, YSZ and pore phases, respectively. Parameters M_{ij} and γ_{ij} are determined based on the physical properties of the Ni–YSZ system. Surface tensions of Ni and YSZ are determined to

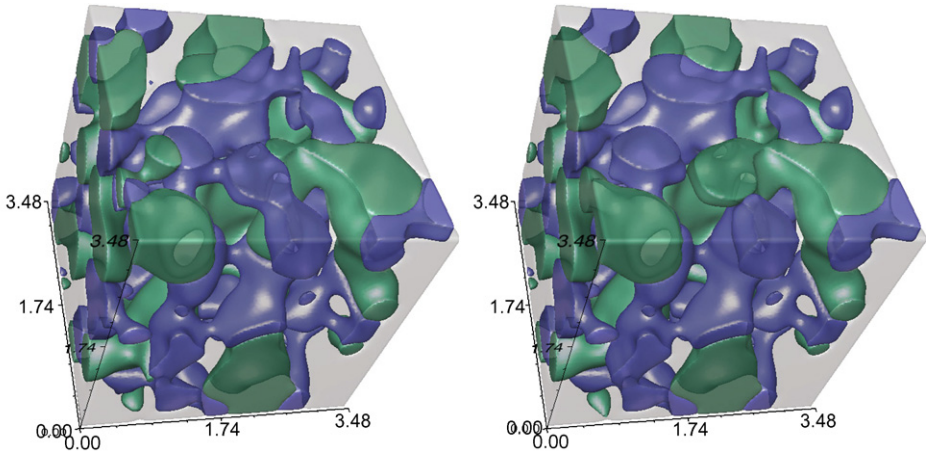

Fig. 2. A comparison of the three phase anode before (left) and after (right) coarsening for 100 h for the reference case using Model B. The Ni, pore, and YSZ phases are represented in green, blue, and semi-transparent, respectively (with volume fractions 24.2%, 20%, and 55.8%, respectively). The TPB density reduced by 23% after coarsening.

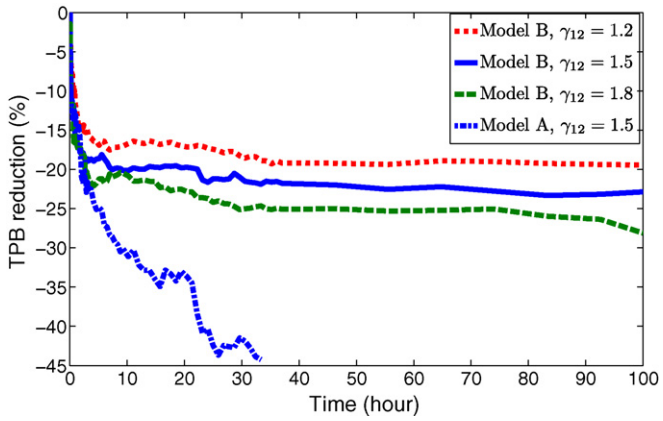

Fig. 3. A comparison of the TPB reduction between Model A and Model B for the reference case, as well as for three different Ni–YSZ interfacial energies using Model B.

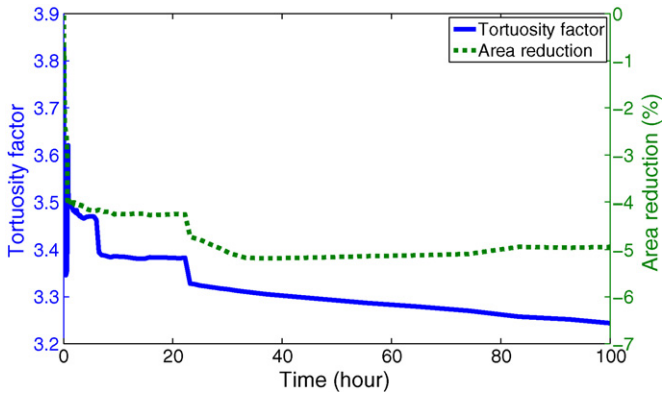

Fig. 4. The evolution of the tortuosity factor and the interfacial area reduction of the pore phase predicted by Model B.

be $\gamma_{13} \cong 1.9\,\mathrm{J\,m^{-2}}$ and $\gamma_{23} \cong 1.4\,\mathrm{J\,m^{-2}}$ [22], and surface diffusivity of them are $D_{13} \cong 3 \times 10^{-10}\,\mathrm{m^2\,s^{-1}}$ [10,11] and $D_{23} \cong 3 \times 10^{-16}\,\mathrm{m^2\,s^{-1}}$ [12]. We estimate the interfacial tension of Ni–YSZ interface to be $\gamma_{12} = 1.5\,\mathrm{J\,m^{-2}}$ [23,24] and use $D_{12} = 3 \times 10^{-20}\,\mathrm{m^2\,s^{-1}}$, respectively. Therefore, we choose $M_{13}{:}M_{23}{:}M_{12} = 1{:}10^{-6}{:}10^{-10}$ and $\gamma_{13}{:}\gamma_{23}{:}\gamma_{12} = 1.9{:}1.4{:}1.5$ as the reference case, using a mobility scale of $3 \times 10^{-10}\,\mathrm{m^2\,s^{-1}}$ and an energy scale of $1\,\mathrm{J\,m^{-2}}$.

A comparison of the anode microstructure before and after coarsening for 100 h using Model B is shown in Fig. 2. The evolution of the microstructure appears to be confined within a short range. Note there are a few regions where YSZ structure appears to change, but they are visualization artifacts. As shown in Fig. 3, Model B predicts that the three-phase boundary (TPB) length becomes nearly constant after coarsening for tens of hours, while Model A indicates that the TPB continues to decrease slowly after a rapid early evolution. These results suggest that Ni phase can be trapped in metastable states if YSZ is immobile. Interestingly, the TPB reduction during the early stage of coarsening are very similar for both models.

For the reference case, the overall TPB reduction after 100-h coarsening was found to be 23% for Model B. A preliminary experimental result for the corresponding case was found to be approximately 26% [25], which is within the uncertainties associated with the simulation. Sources of uncertainties include the values of diffusivities (which change the time scale), the interfacial/surface energies (which change the morphological evolution as well as the time scale), statistical variation of the microstructure in the selected volume, and possible initial smoothing of very small unresolved structures. TPBs in Model A reduced by 44% after 33-h coarsening, and thus it overestimates the reduction significantly. This overestimation is mainly due to the fact that the mobility function we used can introduce excess mobility at triple junctions even with the cutoff, especially when the mobilities differ by orders of magnitude as in the present case.

3.3. Effects of contact angles at triple junctions on anode stability

A parametric study of three different Ni–YSZ interfacial energies (leading to three different sets of contact angles) is performed using Model B. As shown in Fig. 3, the general trend of the coarsening behavior remains the same for all parameter sets. However, TPBs stabilize at an earlier time with less reduction when the Ni–YSZ interfacial energy is smaller, which corresponds to a smaller contact angle of Ni on YSZ. Therefore, such a case is found to be advantageous in preserving TPBs in the Ni–YSZ anode. This result indicates that there is an opportunity for improving the long-time performance of SOFC anodes by controlling the surface/interfacial energies of materials, which can be accomplished, for example, by doping Ni with additives [22].

3.4. Effects of coarsening on pore phase tortuosity

The pore phase in SOFC anodes facilitates the transport of hydrogen. Tortuosity through the pore microstructure allows us to characterize the overall transport property, and it can be used in modeling the electrochemical performance of anodes via macro-homogeneous models [26]. However, tortuosity is difficult to determine experimentally. Therefore, using the microstructures evolved by Model B, we examine the evolution of the tortuosity factor determined as described in [5,27], averaged over three orthogonal directions, and the interfacial area of the pore phase over 100 h of coarsening. As can be seen in Fig. 4, the tortuosity variation is correlated to the interfacial area changes during the late evolution; however, this is not necessarily true in the early stage. The transport in the pore phase is thus not solely affected by the average length scale, which is defined here as the inverse of the surface area per unit volume. Our results suggest that coarsening for a significant amount of time may have positive effects on the gas transport in the pore phase.

4. Conclusions

In conclusion, we present the framework of a phase-field approach to quantitatively model Ni coarsening in SOFC Ni–YSZ anodes. Two models are presented—Model A permits limited YSZ mobility while Model B assumes YSZ to be immobile. Although our models contain approximations and the simulation results may be affected by uncertainty in material properties, we find a reasonable agreement of the TPB reduction trend between coarsening experiments and simulations using Model B. Model A, however, overestimates the TPB reduction due to the evolution of the YSZ structure induced by an excess mobility at triple junctions contained in the model. Our simulations show that the major portion of TPB reduction occurs in the early stage of coarsening, and stability of TPBs is observed provided that YSZ is stationary. Furthermore, we demonstrate that smaller Ni–YSZ interfacial energy can enhance the stability of the TPB density. These models can be extended to simulate other operating conditions of SOFCs. Moreover, the framework of Model B can be applied to solve other physical problems when the wetting condition plays an important role.

Acknowledgements

The work was supported by the National Science Foundation, Ceramics Program under Grant Numbers DMR-0907030/DMR-0542619 (University of Michigan) and DMR-0907639/DMR-0542740 (Northwestern University).

References

[1] K.N. Toft, D. Lybye, M. Mogensen, C. Hatchwell, in: S. Linderoth, et al. (Eds.), Solid State Electrochemistry, Proceedings of the 26th Riso International Symposium on Materials Science, Risø National Laboratory, 2005, pp. 291–296.
[2] D. Simwonis, F. Tietz, D. Stover, Solid State Ionics 132 (2000) 241–251.
[3] P. Tanasini, M. Cannarozzo, P. Costamagna, A. Faes, J.V. Herle, A. Hessler-Wyser, C. Comninellis, Fuel Cells 9 (2009) 740–752.
[4] S. Jiang, J. Mater. Sci. 38 (2003) 3775–3782.
[5] J.R. Wilson, W. Kobsiriphat, R. Mendoza, H. Chen, J.M. Hiller, D.J. Miller, K. Thornton, P.W. Voorhees, S.B. Adler, S.A. Barnett, Nat. Mater. 5 (7) (2006) 541–544.
[6] A.K.A. Ioselevich, W. Lehnert, J. Electrochem. Soc. 144 (9) (1997) 3010.
[7] R. Vaβen, D. Simwonis, D. Stover, J. Mater. Sci. 36 (2001) 147.
[8] J.H. Kim, W.K. Liu, C. Lee, Comput. Mech. 44 (2009) 683–703.
[9] A.I. Zaitsev, N.E. Zaitseva, High Temp. 40 (2) (2002) 197–202.
[10] J.M. Blakely, H. Mykura, Acta Metall. Mater. 9 (1961) 23–31.
[11] P. Maiya, J. Blakely, J. Appl. Phys. 38 (1967) 698.
[12] W.F. Gale, T.C. Totemeier, Smithells Metals Reference Book, 8th ed., Elsevier, 2004.
[13] D.J. Seol, S.Y. Hu, Z.K. Liu, S.G. Kim, K.H. Oh, L.Q. Chen, J. Appl. Phys. 98 (2005) 044910.
[14] R. Folch, M. Plapp, Phys. Rev. E 72 (2005) 011602-1.
[15] S.M. Wise, J.S. Lowengrub, J.S. Kim, W.C. Johnson, Superlattices Microstruct. 36 (2004) 293–304.
[16] D.-H. Yeon, P.-R. Cha, M. Grant, Acta Mater. 54 (2006) 1623–1630.
[17] J.A. Warren, T. Pusztai, L. Kornyei, L. Gransay, Phys. Rev. B 79 (2009) 014204.
[18] L. Granasy, T. Pusztai, D. Saylor, J.A. Warren, Phys. Rev. Lett. 98 (2007) 035307.
[19] H.-C. Yu, H.-Y. Chen, K. Thornton, arXiv:0912.1288.
[20] A. Bueno-Orovio, V.M. Perez-Garcia, Numer. Meth. Part D E 22 (2006) 435–448.
[21] X. Li, J. Lowengrub, A. Ratz, A. Voigt, Commun. Math. Sci. 7 (2009) 81–107.
[22] A. Tsoga, A. Naoumidis, P. Nikolopoulos, Acta Mater. 44 (9) (1996) 3679–3692.
[23] A. Christensen, E. Carter, J. Chem. Phys. 114 (13) (2001) 5816–5831.
[24] J. Beltran, S. Gallego, J. Cerda, J. Moya, M. Munoz, Phys. Rev. B 68 (2003) 075401.
[25] J. Wilson, J. Cronin, S. Barnett, Scr. Mater., submitted.
[26] S. DeCaluwe, H. Zhu, R. Kee, G. Jackson, J. Electrochem. Soc. 155 (6) (2008) B538–B546.
[27] H.-Y. Chen, Y. Kwon, K. Thornton, Scr. Mater. 61 (2009) 52–55.